Physica 11D (1984) 324–336
North-Holland, Amsterdam

SCATTERING OF REGULARIZED-LONG-WAVE SOLITARY WAVES

P.J. MORRISON*, J.D. MEISS and J.R. CARY
Institute for Fusion Studies, The University of Texas at Austin, Austin, Texas 78712, USA

Received 26 April 1983
Revised 1 December 1983

The Lagrangian density for the regularized-long-wave equation (also known as the BBM equation) is presented. Using the trial function technique, ordinary differential equations that describe the time dependence of the position of the peaks, amplitudes, and widths for the collision of two solitary waves are obtained. These equations are analyzed in the Born and "equal-width" approximations and compared with numerical results obtained by direct integration utilizing the split-step fast Fourier-transform method. The computations show that collisions are inelastic and that production of solitary waves may occur.

1. Introduction

The regularized-long-wave (RLW) equation was first obtained by Peregrine [1] to describe the development of an undular bore; i.e, a smooth solitary wave that is observed to propagate in shallow water channels. Since then, the RLW equation has been used as a one-dimensional model for drift waves in plasmas [2]. It is also appropriate to describe Rossby waves in geophysics.

Benjamin et al. [3] proposed the RLW equation as a numerically superior modification of the Korteweg–deVries (KdV) equation. This superiority arises because, unlike the KdV equation, the dispersion relation associated with the linearized RLW equation yields a frequency that is bounded for large wavenumbers. (It has been noted [4] that this numerical advantage is obtained at the expense of precision in the asymptotics.) In spite of this numerical advantage, the RLW equation is not integrable by the inverse scattering transform, and inelasticity has been observed in computations of solitary wave collisions [2, 5]. Also, it is known to possess only a finite number of polynomial conservation laws [6, 7].

*Also Department of Physics,

In this paper we present detailed analyses of the scattering of solitary waves of the RLW equation. Since the RLW equation is not integrable, we do not have exact methods at our disposal. Instead, we must develop approximate analytical techniques and numerical methods.

Our approximate analytical techniques are based on the field Lagrangian, from which the RLW equation is obtained by variation. The Lagrangian approach provides a natural basis for interpretation and analysis. For example, straightforward application of Noether's theorem (in section 2) yields the conserved quantities that correspond to the mass, momentum, and energy of the field. Insertion of the solitary wave solution into the Lagrangian (in section 3) allows us to assign mass, momentum, and energy to solitary waves. As in Hamiltonian mechanics, the solitary wave speed is given by the derivative of the energy with respect to momentum. Knowledge of these invariants also provides rigorous information concerning the outcome of collisions of solitary waves.

For a detailed analysis of solitary-wave collisions, we use a trial function or Rayleigh–Ritz method [8] (in section 4). The simplest trial function corresponds to a sum of two solitary-wave

solutions, where all of the parameters describing the solitary waves are allowed to vary in time. Variation of the Lagrangian with respect to these parameters yields six first-order ordinary differential equations that describe the collision.

As expected, this perturbation technique describes the collision only when the actual solution has a form not too different from the trial function. Some improvement might be obtained by allowing the parameters to depend slowly on space or adding more variational parameters. As we will see below however, when the trial function method fails, it fails catastrophically, and this could hardly be remedied by the addition of a slow spatial modulation.

The ordinary differential equations describing the collision can be solved using the Born approximation of particle scattering theory. Unfortunately the agreement of this approximate solution with subsequent numerical calculations is not good, even when the relative speeds are large, where good agreement is obtained in ordinary classical particle scattering. The reason can be traced to the nature of the interaction potential. For ordinary particle collisions, the potential is fixed, and so it becomes relatively less important as the center of mass energy is increased. In contrast, the interaction potential for solitary waves increases with increasing speed. Hence, there is no regime in which the interaction potential is relatively small.

This limitation of the Born approximation motivates us to develop an alternate, high-energy approximation based on the use of the high-energy asymptotic formulas for the solitary-wave parameters. For example, the width of the solitary wave asymptotes to a constant in the high-energy limit. This approximation allows us to solve our set of differential equations by quadratures.

Further, this approximation motivates us to derive (in section 5) an equation for which the high-energy solitary wave relations of the RLW equation are rigorously valid at all energies. With this equation, we can compare three separate solutions to determine whether observed inaccuracies, if any, are due to the use of the asymptotic solitary wave solutions as trial functions for the RLW equation, or to some more basic assumption of the trial function method.

To check our analytic results, we numerically integrate the partial differential equations in section 6. The trial function method, when applied to collisions of solitary waves moving in the same direction, is in excellent agreement with the completely numerical solution. Unfortunately, accurate results are not obtained for collisions of oppositely-directed solitary waves.

Part of this inaccuracy is due to the gross inelasticity observed in low to medium energy collisions. The numerical solutions show that for a certain region of the parameter space of scattering, two additional solitary waves can be produced in the collision. It is interesting that the Born approximation predicts a peak in the phase shift in this region of parameter space.

However, even when the energies are large but oppositely directed, in which case the collisions are nearly elastic, the trial function method does not give accurate predictions for the outcome of the scattering. We therefore conclude that the trial function introduced in section 4 provides an inadequate representation of the colliding solitary waves. Thus, more complicated trial functions are needed to describe the interaction of forward and backward solitary waves.

2. Field Lagrangian

The RLW equation is [2]

$$\phi_t - \phi_{xxt} + \phi_x - \phi\phi_x = 0, \tag{1}$$

for a field $\phi(x, t)$. In the fluid problem ϕ is related to the negative of the vertical displacement of the water surface, while in the plasma application ϕ is the electrostatic potential. A variational form is obtained by analogy with the KdV equation by representing ϕ in terms of a "potential", ψ; i.e.,

$\phi = \psi_x$. The action is written as a functional of ψ,

$$A[\psi] = \int_{-\infty}^{\infty} dt\, L[\psi, \psi_t] = \int_{-\infty}^{\infty} dt \int_{-\infty}^{\infty} dx\, \mathscr{L}(\psi_x, \psi_t, \psi_{xt}, \psi_{xx}), \quad (2)$$

where the Lagrangian density is

$$\mathscr{L} = \tfrac{1}{2}\left(\tfrac{1}{3}\psi_x^3 - \psi_x^2 - \psi_x\psi_t - \psi_{xx}\psi_{xt}\right). \quad (3)$$

Variation of eq. (2) yields

$$\frac{\delta A}{\delta \psi} = \psi_{xt} - \psi_{xxxt} + \psi_{xx} - \psi_x\psi_{xx},$$

from which solutions to the RLW equation are seen to be extremal functions for eq. (2).

Constants of the motion may be obtained from the Lagrangian by straightforward application of Noether's theorem [8]. Form invariance of the Lagrangian for a shift of ψ, $L(\psi, \psi_t) = L(\psi + \epsilon, \psi_t)$, shows that the mass,

$$\mathscr{M} \equiv -\int dx\, \frac{\delta L}{\delta \psi_t} = \tfrac{1}{2}\int dx\, \phi, \quad (4)$$

is an invariant of the motion. Similarly, form invariance of the Lagrangian with respect to space and time translation, shows that the momentum,

$$\mathscr{P} \equiv -\int dx\, \frac{\delta L}{\delta \psi_t}\frac{\partial \psi}{\partial x} = \tfrac{1}{2}\int dx\, (\phi^2 + \phi_x^2), \quad (5)$$

and energy

$$\mathscr{E} \equiv \int dx \left(\frac{\delta L}{\delta \psi_t}\psi_t - L\right) = \tfrac{1}{2}\int dx\, (\phi^2 - \tfrac{1}{3}\phi^3). \quad (6)$$

are invariants, respectively. These are the only polynomial constants of the motion [6, 7].

3. Solitary waves

The RLW equation is known to have solitary wave solutions of the form

$$\phi(x,t) = \phi_s(A, k, x - \theta) \equiv A(t)\,\mathrm{sech}^2\{k(t)[x - \theta(t)]\}. \quad (7)$$

The relation between the constants A, k and the speed, $\dot{\theta}$, is easily obtained by direct substitution of eq. (7) into eq. (1). As an introductory example of the trial function method, we demonstrate how this solution follows from insertion of ϕ_s into the Lagrangian and variation with respect to general functional dependences of A, k, and θ on time. Insertion of eq. (7) into eq. (2) and performing the spatial integrations yields

$$L(A,k,\theta) = \left[\dot{\theta}\left(\frac{2A^2}{3k} + \frac{8}{15}A^2k\right) - \frac{2A^2}{3k} + \frac{8A^3}{45k}\right], \quad (8)$$

which gives the equations of motion

$$\frac{d}{dt}\left(\frac{2A^2}{3k} + \frac{8}{15}A^2k\right) = 0, \quad (9a)$$

$$\dot{\theta}\left(\frac{2A^2}{3k^2} - \frac{8A^2}{15}\right) + \left(-\frac{2A^2}{3k^2} + \frac{8}{45}\frac{A^3}{k^2}\right) = 0, \quad (9b)$$

$$\dot{\theta}\left(\frac{4A}{3k} + \frac{16Ak}{15}\right) + \left(\frac{-4A}{3k} + \frac{8A^2}{15k}\right) = 0. \quad (9c)$$

These equations can be used to derive unique relations among the soliton parameters,

$$A = \frac{12k^2}{4k^2 - 1}, \quad (10)$$

$$c \equiv \dot{\theta} = (1 - 4k^2)^{-1}, \quad (11)$$

where A, k and c are constant.

Eqs. (10) and (11) can be solved to find the solitary wave amplitude and width in terms of its speed,

$$k = \tfrac{1}{2}(1 - c^{-1})^{1/2}, \quad (12a)$$

$$A = 3(1 - c). \quad (12b)$$

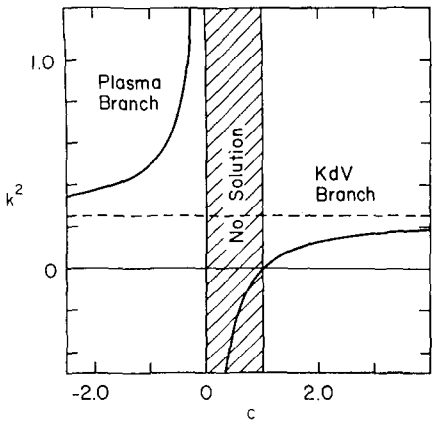

Fig. 1. The function $k^2(c)$ as given by eq. (13). Bounded solutions of RLW have $k^2 > 0$.

Fig. 1 displays the relation of eq. (12a). Two branches are observed. For $c > 1$, A is negative. These solitary waves resemble the single soliton solution to the KdV equation (particularly when c is slightly larger than unity). It is this branch that models the undular bore (note that A is the negative of the fluid displacement). The other branch occurs for $c < 0$, for which A is positive. This branch is not applicable to the surface waves but is relevant in plasma physics (see ref. 2). For $0 < c < 1$, k is imaginary, hence the solutions are unbounded (and undesirable).

Substitution of eq. (7) into the expressions in eqs. (4)–(6) for mass, momentum, and energy yields

$$M \equiv \mathcal{M}(\phi_s) = \frac{A}{k}, \tag{13a}$$

$$P \equiv \mathcal{P}(\phi_s) = \frac{2A^2}{3k}\left(1 + \frac{4k^2}{5}\right), \tag{13b}$$

$$H \equiv \mathcal{E}(\phi_s) = \frac{2A^2}{3k}\left(1 - \frac{4A}{15}\right). \tag{13c}$$

In fig. 2 we plot these invariants as functions of the solitary wave speed. Observe the momentum threshold necessary for the existence of solutions with negative speed.

Comparing eqs. (13) and (8), we obtain

$$L(A, k, \theta) = \dot{\theta}P - H. \tag{14}$$

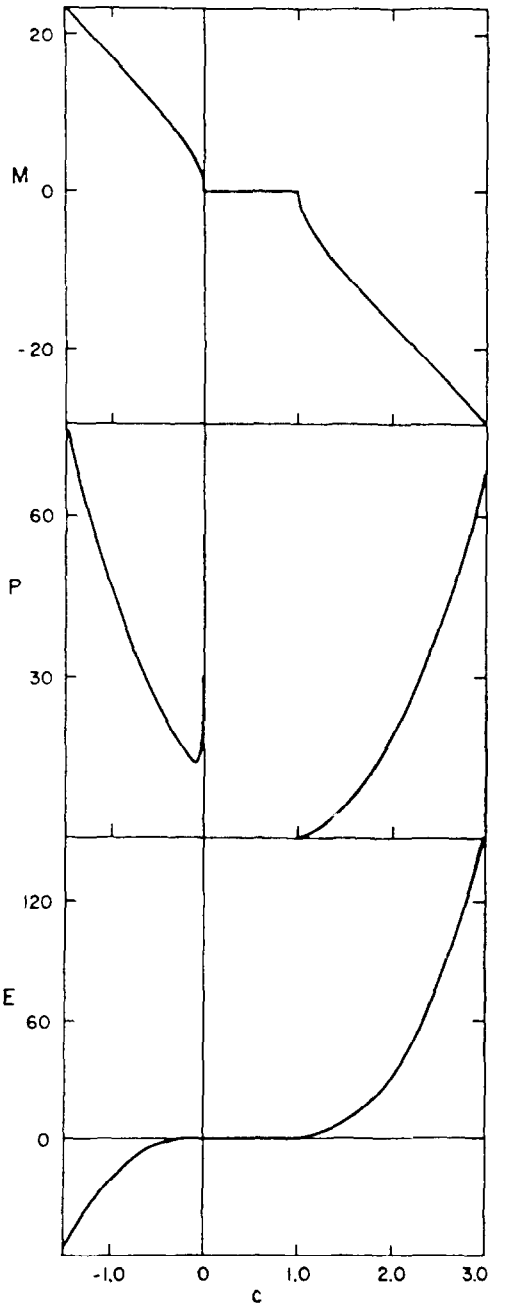

Fig. 2. Mass, momentum, and energy of the solitary wave solution to RLW from eq. (14).

If we assume from the outset the relationship eq. (10) between k and A, then eq. (14) becomes

$$L(P, \theta) = \dot{\theta}P - H(P), \tag{15}$$

which is clearly seen to be the variational principle that produces Hamilton's equations with θ canonically conjugate to P. In this case θ is ignorable. Note that the derivative of the energy with respect to the momentum gives the speed of the solitary wave.

4. Solitary wave collisions

To analyze solitary wave collisions with the trial function method, we must choose a suitable trial function. The trial function must reduce to the linear superposition of separated solitary waves at large positive and negative times, yet it must allow the solitary waves to interact when they are close. The linear superposition of the two solitary waves,

$$\phi = \phi_1 + \phi_2, \tag{16}$$

with

$$\phi_i = \phi_s(A_i, k_i, x - \theta_i), \tag{17}$$

satisfies these criteria. This form can only work when the collision is nearly elastic, since it ignores production of radiation or solitons. We will see that this is valid in some parameter regimes, but fails in others.

Substitution of eq. (16) into eq. (2) yields

$$\begin{aligned} L = {} & L_1(A_1, k_1, \dot{\theta}_1) + L_2(A_2, k_2, \dot{\theta}_2) \\ & + L_{12}(A_1, k_1, A_2, k_2, \theta_1 - \theta_2; \\ & \dot{A}_1, \dot{A}_2, \dot{k}_1, \dot{k}_2, \dot{\theta}_1, \dot{\theta}_2), \end{aligned} \tag{18}$$

where

$$L_i = p_i\dot{\theta}_i - H_i, \tag{19}$$

$$p_i \equiv \mathscr{P}[\phi_i], \tag{20}$$

$$H_i(p_i, k_i) \equiv \mathscr{E}[\phi_i]. \tag{21}$$

It no longer follows that the individual momenta and energies are conserved. However, the interaction Lagrangian, L_{12}, is a function of the difference between θ_1 and θ_2 (by translational invariance) and vanishes as $|\theta_1 - \theta_2| \to \infty$. Thus, in this limit, the solitary waves obey the free equations of motion. The only effect of the collision is a phase shift, $\Delta\theta_i$, which represents the difference between the actual θ and its free value

$$\Delta\theta_i = \lim_{t\to\infty} \left[\theta_i(t) - c_i t - \theta_i(0)\right]. \tag{22}$$

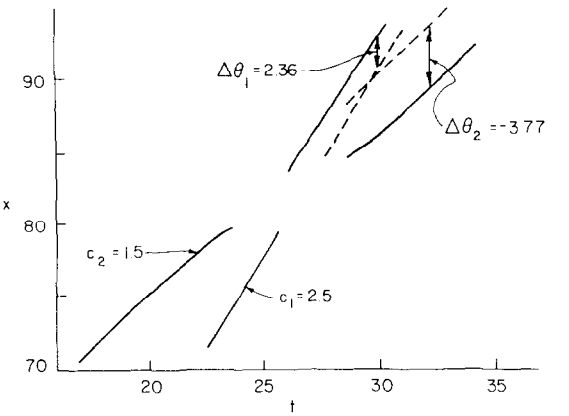

Fig. 3. Trajectories of the peaks of two solitary waves for RLW. For several units of time the peak corresponding to c_2 vanishes. This collision is nearly elastic.

An example of the trajectories of the solitary wave peaks for an actual collision and resulting phase shifts (see section 5) are shown on fig. 3.

The phase shifts may be calculated by solving the equations of motion resulting from eq. (18). As these are complicated, we resort to approximation.

4.1. *Born approximation*

If we eliminate A_i in lieu of p_i in eq. (18), then the equations of motion take the form

$$\begin{aligned} \dot{\theta}_1 - \frac{\partial H_1}{\partial p_1} &= -\frac{\partial L_{12}}{\partial p_1} + \frac{\mathrm{d}}{\mathrm{d}t}\frac{\partial L_{12}}{\partial \dot{p}_1}, \\ \dot{p}_1 &= \frac{\partial L_{12}}{\partial \theta_1} - \frac{\mathrm{d}}{\mathrm{d}t}\frac{\partial L_{12}}{\partial \dot{\theta}_1}, \\ \frac{\partial H_1}{\partial k_1} &= \frac{\partial L_{12}}{\partial k_1} - \frac{\mathrm{d}}{\mathrm{d}t}\frac{\partial L_{12}}{\partial \dot{k}_1}, \end{aligned} \tag{23}$$

and similarly for $i = 2$. The phase shift is obtained by integrating over the deviation due to the inter-

action term,

$$\Delta\theta_1 = \int_{-\infty}^{\infty} \mathrm{d}t \left(\dot{\theta}_1 - \frac{\partial H_1}{\partial p_1} \right) = - \int_{-\infty}^{\infty} \mathrm{d}t \, \frac{\partial L_{12}}{\partial p_1}. \tag{24}$$

To lowest order, assuming the interaction is small, eq. (24) is evaluated by integrating along unperturbed trajectories,

$$\Delta\theta_1 = - \int_{-\infty}^{\infty} \mathrm{d}t \, \frac{\partial L_{12}}{\partial p_1} [\, p_1, k_1, p_2, k_2, \theta_{10} - \theta_{20} + (c_1 - c_2)t], \tag{25}$$

where θ_{i0} is the peak position at $t = 0$. Changing variables, eq. (25) becomes

$$\Delta\theta_1 = \frac{-1}{c_1 - c_2} \frac{\partial}{\partial p_1} \int_{-\infty}^{\infty} \mathrm{d}y \, L_{12}(p_1, k_1, p_2, k_2, y). \tag{26}$$

The interaction Lagrangian is

$$L_{12} = - \int_{-\infty}^{\infty} \mathrm{d}x \, (\phi_1 \psi_{2t} + \phi_{1x}\phi_{2t} + \phi_1\phi_2 - \tfrac{1}{2}\phi_1\phi_2^2 - \tfrac{1}{2}\phi_1^2\phi_2). \tag{27}$$

With eq. (27) we see that the form of the double integral in eq. (26) is particularly easy to evaluate. For example, consider the evaluation of the second term,

$$- \int_{-\infty}^{\infty} \mathrm{d}y \int_{-\infty}^{\infty} \mathrm{d}x \, \phi_{1x}\phi_{2t} = - \int_{-\infty}^{\infty} \mathrm{d}y \int_{-\infty}^{\infty} \mathrm{d}x \, \frac{\partial \phi_s}{\partial x}(A_1, k_1, x - y) \times \frac{\partial \phi_s}{\partial x}(A_2, k_2, x)\dot{\theta}_2.$$

Upon interchanging the order of integration, we find that this term vanishes. Similarly, the first term vanishes. Integration of the remaining terms gives

$$- \int_{-\infty}^{\infty} L_{12} \, \mathrm{d}y = 4\frac{A_1 A_2}{k_1 k_2} - \frac{A_1 A_2}{k_1 k_2}(A_1 + A_2). \tag{28}$$

Using eq. (28) in eq. (26), we obtain by implicit differentiation

$$\Delta\theta_1 = \frac{A_2(6 - A_2 - 2A_1)}{2A_1(c_1 - c_2)k_2(1 + 4k_1^2/5)}. \tag{29}$$

The formula for $\Delta\theta_2$ is obtained by interchanging 1 and 2.

In spite of the simplicity of the Born approximation, one cannot rely on it too heavily. The reason is the breakdown of the approximation made in using the unperturbed trajectories. During the interaction, the velocity of the first solution varies from its noninteracting value by a quantity of order $\Delta c_1 \approx \Delta\theta_1/\Delta t$, where $\Delta t = (k_1^{-1} + k_2^{-1})/|c_1 - c_2|$ is the interaction time. The Born approximation requires $\Delta c_1 \ll c_1$, or

$$\left| \frac{\Delta\theta_1(c_1 - c_2)}{c_1(k_1^{-1} + k_2^{-1})} \right| \ll 1.$$

A similar condition for the second soliton is obtained by interchanging indices, $1 \leftrightarrow 2$. Use of eq. (29) reduces this inequality to

$$\left| \frac{A_2(6 - A_2 - A_1)}{2A_1c_1(1 + k_2/k_1)(1 + 4k_1^2/5)} \right| \ll 1.$$

This condition and its companion obtained by interchanging the indices are marginally satisfied in some regimes, but well-satisfied nowhere. Thus, we can expect at most only qualitative agreement between the Born approximation and numerically obtained results.

4.2. *Large amplitude approximation*

The Born approximation fails over much of the collision parameter space, because the predicted phase shifts are large and the trajectories strongly perturbed. However, direct calculation of the trajectories is difficult due to the complicated form of the interaction potential in the Lagrangian. This potential can be greatly simplified by considering

collisions of large amplitude (velocity) solitary waves for which the widths, from eq. (12a), are nearly equal. As seen in fig. 1, when $k = \frac{1}{2} \pm \varepsilon$, ($\varepsilon \ll 1$) the speed is large and negative (positive).

To utilize this approximation, we set $k_i = 1/2 + 3/4a_i$ with $|a_i| \gg 1$ and enforce the $A(k)$ relationship, eq. (10). The amplitude is given by $A_i = a_i + \mathcal{O}(1)$ and the leading order terms in L will be $\mathcal{O}(a_i^3)$.

Due to the widths of the two solitary waves being almost equal, the Lagrangian can be obtained in terms of a single integral

$$I(y) \equiv \int_{-\infty}^{\infty} \operatorname{sech}^2 z \tanh(z-y)\,\mathrm{d}z = 2\left[\frac{\cosh y \sinh y - y}{\sinh^2 y}\right], \tag{30}$$

where $y = (\theta_1 - \theta_2)/2$. Scaling L by a factor of $8/5$, we obtain from eqs. (18) and (27)

$$\frac{5}{8}L = \sum_{i=1}^{4} \dot{z}^i f_i(z) - H(z), \tag{31}$$

where

$$z = \begin{pmatrix} \theta_1 \\ \theta_2 \\ a_1 \\ a_2 \end{pmatrix}, \quad f = \begin{bmatrix} a_1^2 - a_1 a_2 J'(y) \\ a_2^2 - a_1 a_2 J'(y) \\ -2a_2 J(y) \\ 2a_1 J(y) \end{bmatrix}; \tag{32}$$

$$H(z) = (2/3)a_1 a_2 (a_1 + a_2) J'(y) - (2/9)(a_1^3 + a_2^3); \tag{33}$$

$$J(y) \equiv \frac{5}{32}\left(-4 + \frac{\partial^2}{\partial y^2}\right) I(y). \tag{34}$$

For reference, we note that J is an odd function with asymptotes $J(\pm\infty) = \mp 5/4$, and $J(y) = -y + 4y^3/21 - 4y^5/105 + \mathcal{O}(y^7)$.

The Lagrangian has been written in standard form so that the equations of motion become

$$\Omega \cdot \dot{z} = \frac{\partial H}{\partial z}, \qquad \Omega_{ij} \equiv \frac{\partial f_j}{\partial z_i} - \frac{\partial f_i}{\partial z_j}, \tag{35}$$

where Ω is the antisymmetric two-form. To solve eq. (35), we must invert Ω, obtaining the components of the cosymplectic form $J = \Omega^{-1}$. This requires nondegenerate Ω. The determinant is

$$\det \Omega = 16 a_1^2 a_2^2 F^2, \qquad F = 1 + JJ'' - J'^2. \tag{36}$$

The function F has asymptotes $F(\pm\infty) = 1$ and $F(y) = 40y^4/147 + \mathcal{O}(y^6)$. Thus, we see that det Ω vanishes only at $y = 0$.

Since Ω is a closed, nondegenerate two-form, it is possible (Darboux's theorem) to transform the equations of motion into canonical form with H being the Hamiltonian. This system then has two degrees of freedom. Furthermore, the system is completely integrable, since mass and momentum as well as energy are conserved. These conserved quantities may be obtained by evaluating eqs. (5)–(7) with the trial function, giving

$$m = \tfrac{1}{2}(a_1 + a_2) = \tfrac{1}{4}\mathcal{M}[\phi_1 + \phi_2],$$
$$p = a_1^2 + a_2^2 - 2a_1 a_2 J' = (5/8)\mathcal{P}[\phi_1 + \phi_2], \tag{37}$$
$$h = (5/8)\mathcal{E}[\phi_1 + \phi_2] + \mathcal{O}(a^2).$$

While canonical coordinates do not appear especially useful, it is convenient to transform to coordinates that include the conserved quantities m and p. Thus, we define $\bar{z} = (y, m, R, p)$ with $y = (\theta_1 - \theta_2)/2$ and $R = (\theta_1 + \theta_2)/2$. The cosymplectic form transforms as

$$\bar{J}^{ij} = \frac{\partial \bar{z}^i}{\partial z^k} J^{kl} \frac{\partial \bar{z}^j}{\partial z^l}$$

and becomes

$$\bar{J}=\frac{1}{a_1a_2F}\times\begin{bmatrix} 0 & (a_1-a_2)\frac{G}{8} & -\frac{J}{2} & 0 \\ -(a_1-a_2)\frac{G}{8} & 0 & m\frac{G}{4} & 0 \\ \frac{J}{2} & -m\frac{G}{4} & 0 & -a_1a_2F \\ 0 & 0 & a_1a_2F & 0 \end{bmatrix}; \tag{38}$$

where $G=1+J'$, and the Hamiltonian is

$$h(\bar{z})=\frac{8}{9}m^3-\frac{2}{3}mp. \tag{39}$$

The equations of motion $\dot{\bar{z}}=\bar{J}\cdot(\partial h/\partial\bar{z})$ are, besides $\dot{m}=\dot{p}=0$,

$$\dot{y}=-\frac{1}{3}\frac{G^{3/2}}{F}\left(Gm^2-a_1^\infty a_2^\infty\right)^{1/2} \tag{40}$$

and

$$\dot{R}=\tfrac{1}{3}m\left(\frac{G^2}{F}-2\right), \tag{41}$$

where $a_1^\infty a_2^\infty=(4m^2-p)/2$ is the product of the amplitudes when $|y|=\infty$. Note that eq. (40) is an autonomous first-order differential equation. Hence, its solution can be written in terms of integrals.

These equations predict quite different evolution depending on the sign of $a_1^\infty a_2^\infty$. For $a_1^\infty a_2^\infty>0$, there is a distance of closest approach, $y_{\min}$, such that $G(y_{\min})=a_1^\infty a_2^\infty/m^2$ where the square root in eq. (40) vanishes. In the neighborhood of this minimum $y-y_{\min}\propto(t-t_c)^2$, where t_c is the collision time. These collisions are "exchange" collisions: since $\dot{y}(-\infty)=-\dot{y}(\infty)$, the solitary waves exchange identities at $y_{\min}$.

By contrast, when $a_1^\infty a_2^\infty<0$, the square root in eq. (40) is always nonzero and y continues to decrease. Near $y=0$ we can expand the functions G and F to obtain

$$\dot{y}=-\frac{\sqrt{7}}{5}\frac{1}{|y|}\left(-a_1^\infty a_2^\infty\right)^{1/2}+\mathcal{O}(y),$$

which has the solution $y\propto|t_c-t|^{1/2}$ where, as before, t_c is the collision time. In these collisions, the solitary waves maintain their identities.

Anticipating the results of the numerical experiments, we remark that agreement between the trial function equations and the actual partial differential equation is expected to be better for the exchange collisions since the relative forces are smaller when $y>y_{\min}$.

5. The equal width equation

The results of the previous section involve two approximations: that due to the trial function method and the simplifications made in order to handle the interaction Lagrangian. In the second such simplification, the large amplitude approximation, terms of order a_i^2 were neglected. Hence, it is clear that eqs. (40) and (41) could be obtained if from the outset we began with the Lagrangian density

$$\mathscr{L}=\tfrac{1}{2}\left(\tfrac{1}{3}\psi_x^3-\psi_x\psi_t-\psi_{xx}\psi_{xt}\right). \tag{42}$$

Eqs. (40) and (41) involve only the trial function approximation, for the equation obtained by variation using eq. (42).

The equation thus obtained is

$$\phi_t-\phi_{xxt}-\phi\phi_x=0. \tag{43}$$

The equation might be called the equal-width equation (EWE) since it possesses solitary wave solutions of the form of eq. (7), but with

$$k=\tfrac{1}{2},\quad A=-3c. \tag{44}$$

Note that there exist solutions for all values of c, even in the range $0<c<1$.

Like the RLW equation, the EWE possesses

only three polynomial conservation laws [6]. These may be obtained by realizing that the EWE transforms into the RLW under

$$\phi_{\mathrm{EWE}} \to \phi_{\mathrm{RLW}} - 1. \tag{45}$$

Transforming the three RLW constants by the inverse of eq. (45) yields the three independent EWE constants

$$\mathscr{M} = \tfrac{1}{2}\int_{-\infty}^{\infty} \phi(x,t)\,\mathrm{d}x,$$

$$\mathscr{P} = \tfrac{1}{2}\int_{-\infty}^{\infty} \left(\phi^2 + \phi_x^2\right)\mathrm{d}x,$$

$$\mathscr{E} = -\int_{-\infty}^{\infty} \left(\phi^3/6\right)\mathrm{d}x.$$

We observe in section 6 that the numerical solutions of the EWE do not possess a radiation field component. This may be related to the fact that the Fourier transform of the linearized EWE is equivalent to $\omega(1+k^2)=0$ and does not provide any relation between frequency and wavenumber. Furthermore, the solutions of the EWE cannot be simply obtained from those of the RLW equation through eq. (45), since the boundary conditions in the two cases are different.

6. Numerical computations

Numerical solution of the EWE and RLW equation is accomplished by a split-step fast Fourier-transform method [10]. The linear dispersion is solved exactly in Fourier space and the nonlinear terms are advanced by the Lax–Wendorff scheme [11]. Typical computations use 2^{11} grid points and a time step of 0.002. Accuracy has been checked by doubling the number of grid points and halving the time step. Except in the few cases noted below, this makes no observable change.

The primary error in this algorithm is a slow secular drift of the solitary wave speed (and amplitude). In computations involving a single solitary wave, the speed changes by about one percent over $\Delta t = 40$. This secularity has an important effect on phase shift computations.

The phase shifts resulting from a collision are computed from eq. (22). Recall that the variable $\theta_i(t)$ is the position of the peak of the solitary wave. In order to account for the secular change in the speed, we add a constant acceleration term to eq. (22). This effectively replaces the speed by its average; thus

$$\Delta\theta_i = \theta_i(t) - \tfrac{1}{2}\left[c_i(t) + c_i(0)\right]t - \theta_i(0), \quad t \gg t_{\mathrm{c}}, \tag{46}$$

which t_{c} is the collision time.

Another difficulty in the computation of phase shifts arises from the intrinsic inelasticity of the collisions. In a typical collision, some of the momentum is lost to radiation. (We use momentum as a measure of inelasticity because it is positive definite.) Thus, the out-going velocities differ from in-going ones. The use of eq. (46) effectively assumes that this radiation is lost at a constant rate. In any case, we estimate the error in $\Delta\theta$ as that being due to the change in speed.

6.1. *RLW collisions*

We will consider two types of collisions: between two positive velocity or KdV branch solitary waves and between one positive and one negative velocity solitary wave. Most previous studies [5, 12] considered only the first case. Such collisions are nearly elastic and even led researchers to postulate the integrability of the RLW equation. Non-integrability was first observed by Abdullov et al. [5] in a collision with $c_1 = 1.5$ and $c_2 = 3.0$ where radiation with an amplitude of about 0.3% of the solitary wave is produced. Subsequently a careful numerical study by Bona et al. [5] confirmed the radiation production showing that it seems to peak when the smaller solitary wave has about half the amplitude of the larger. Bona et al. observed that the smaller solitary wave loses amplitude while the larger gains amplitude. We have observed the same phenomena, though we use about a factor of seven

fewer grid points making an accurate calculation of this small inelasticity impossible.

More dramatic inelasticity is observed in head-on collisions of RLW solitary waves. Creation of solitary waves in pairs was observed by Santarelli [13], and confirmed by Courtenay Lewis and Tjon [14].

In fig. 4, we display the (c_1, c_2) phase space of two solitary wave collisions for the RLW equation. Since this diagram is symmetric under $c_2 \leftrightarrow c_1$, we need only consider the region above the dashed line, $c_1 = c_2$. The speckled region, where both speeds are nearly equal to one, is well approximated by the KdV equation. Here the collision is nearly elastic. In fact, for all of our computations with both speeds positive, the inelasticity is difficult to detect.

Computations with $c_2 < 0$, where four solitary waves emerge from the initial two, are indicated by the symbol "+" on fig. 4. An example of such a collision is shown in fig. 5. The four solitary pulses, as well as a localized pulse of radiation, are evident at $t = 40$. The trajectories of the peaks are shown in fig. 6, and labelled with the measured speeds. In all cases, the produced solitary waves come in positive-negative pairs, in this case with $c = 1.32$ and -0.37. The shaded region in fig. 6 represents the zone occupied by the radiation. The edges of this zone propagate at roughly the maximum and minimum linear group velocities. Courtenay Lewis and Tjon [14] have observed cases where more than one pair is produced, and even where both initial solitary waves are destroyed.

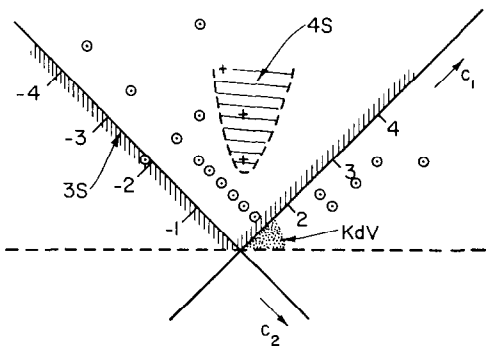

Fig. 4. Collision phase space for RLW. Speeds $0 < c < 1$ are omitted from the graph. Computations are marked by circles when only two solitary waves and radiation are emitted. The plus represents cases for which four solitary waves and radiation are emitted.

Collisions of positive and negative pulses are characterized by the appearance of sharp gradients. For the example of fig. 5, the wavenumber spectrum at the most violent point ($t = 9.6$) peaks at $k \approx 2.3$ with a full width of 3.5; modes with $k > 14$ have amplitudes less than three percent of the peak. The integrator keeps modes with $k \leq 55$ and hence, has no problem resolving this collision.

The shaded region in fig. 4 labelled "4S" is a sketch of the phase space for which production of four solitary waves is observed. If we assume that the emergent solitary waves must come in positive-negative pairs, then conservation of momentum allows an estimate of the lower boundary of the 4S region: the total initial momentum must be great enough to accommodate the production of two negative speed solitary waves. Since there is a momentum threshold for $c < 0$ we have

$$P(c_1) + P(c_2) > 2P_{\min} = 28.$$

The actual threshold seems to be about twice this value (one should, in addition, consider the other two conservation laws).

The region labelled "3S" in fig. 4 is the region for which three solitary waves may be emitted. This region is obtained from the conservation laws, requiring that the energy, momentum and mass of the three out-going solitary waves equal that of the two in-going waves. These three equations have nontrivial solutions for the three velocities (i.e., not replicating the incident speeds) only when one of the initial velocities is in the region $-0.096 < c_2 < 0$, the bifurcation point occurring at $\partial P/\partial c_2 = 0$. The third solitary wave must have positive speed.

Several computations in the "3S" region have not conclusively demonstrated the creation of the third solitary wave. A clear tendency for the creation of a small negative amplitude pulse is seen;

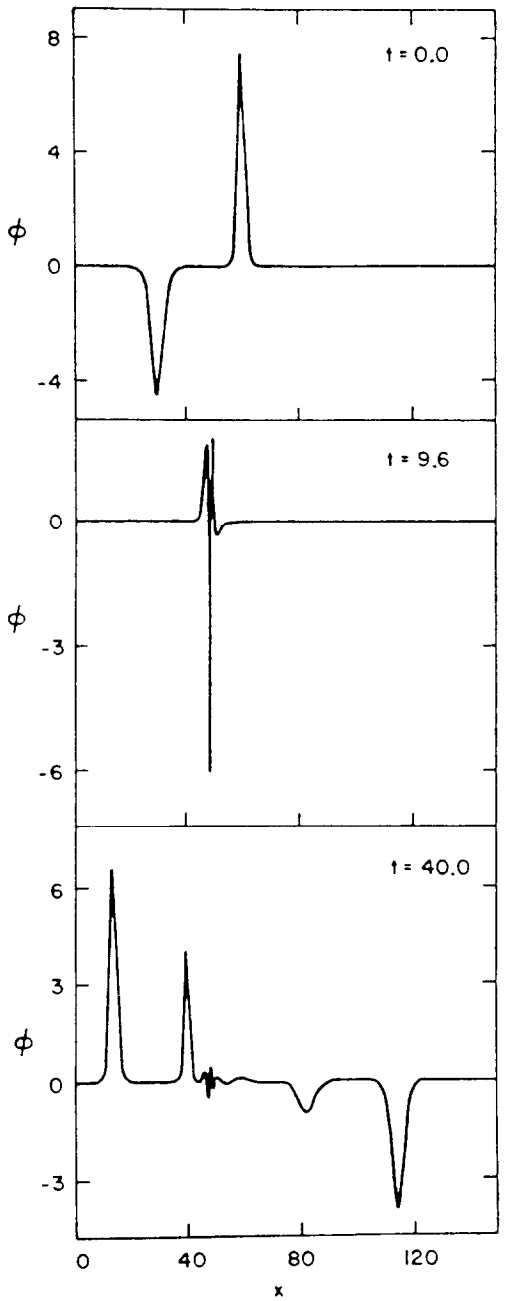

Fig. 5. RLW collision with $c_1 = 2.5$ and $c_2 = -1.5$ showing four solitary waves and radiation in the final state.

however, a considerable amount of radiation is also generated. Computations with solitary waves of very small negative speeds are difficult, since the width goes to zero with c.

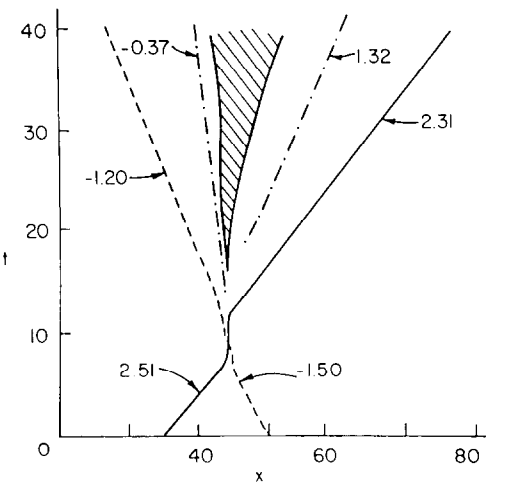

Fig. 6. Trajectories of the peaks for the collision of fig. 5.

Finally, the phase shift calculations of section 4 are compared with numerical computations in fig. 7. Here, the points represent the numerical values of $\Delta\theta$ computed according to eq. (46) for $c_1 = 1.5$ as a function of c_2. The error bars are obtained by using either the initial or final speeds in the computation of $\Delta\theta$; thus giving some measure of the inelasticity. A better indication is the upper graph which shows a plot of the momentum lost by the solitary waves (and hence gained by the radiation) during the collision [14]. Errors in the computation give $\Delta P \approx 3\%$. A large peak in ΔP near $c_2 \approx -0.8$ corresponds also to a peak in both the phase shifts. From fig. 4, it is seen that this phase shift peak corresponds to being near the 4S production threshold. Thus, the phase shift peak is a kind of resonance effect where two new solitary waves are almost created. An example of a collision in this region is shown in fig. 8.

The curves in fig. 7 are computed using the trial function techniques of section 4. For $c_2 < 0$, the displayed curves are given by eq. (29) from the Born approximation. These curves at most qualitatively follow the computed points. It is interesting, however, that the Born approximation for $\Delta\theta_1$ shows a peak at $c_2 \approx -0.8$, in agreement with the computations. For $c_2 > 0$, the Born approximation values for $\Delta\theta$ are too large to fit on the graph. As

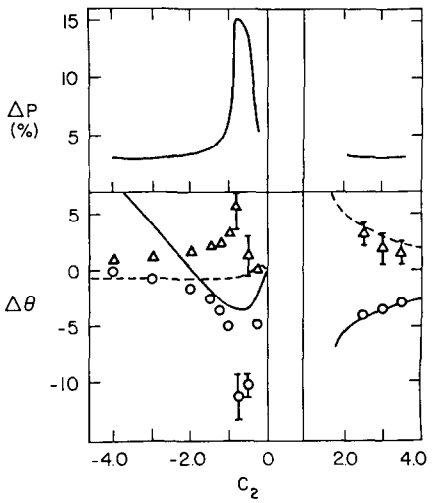

Fig. 7. RLW phase shifts and inelasticity as a function of c_2 for $c_1 = 1.5$, $\Delta\theta_1$ is represented by circles and solid curves, and $\Delta\theta_2$ by triangles and dashed curves. The curves for $c_2 < 0$ are from eq. (29), while for $c_2 > 0$ we use eq. (40)–(41).

discussed, the failure of the Born approximation is due to the relatively large perturbations in the trajectories. The interaction Lagrangian is not small, as assumed in the approximation.

The curves shown in fig. 7 (for $c_2 > 0$) are computed using the large amplitude approximation of section 4.2. The agreement is quantitative. This will be discussed further in the next subsection.

6.2. *EWE collisions*

The large amplitude trial function approximation should work best for the EWE, since here the single solitary wave is exact. Fig. 9 shows the phase shifts computed for the EWE collisions as compared with eqs. (40) and (41). The agreement is very good for $c_2 > 0$ and extremely poor for $c_2 < 0$. Note that the phase shift goes to infinity logarithmically near $c_2 = c_1$.

As noted, collisions with $a_1 a_2 > 0$ are exchange collisions, with the solitary distance always larger than $y_{\min}$. An example is shown in fig. 10. Here, the points are from the numerical experiment and the curves are trajectories obtained from eqs. (40) and (41). Though the comparison is difficult near

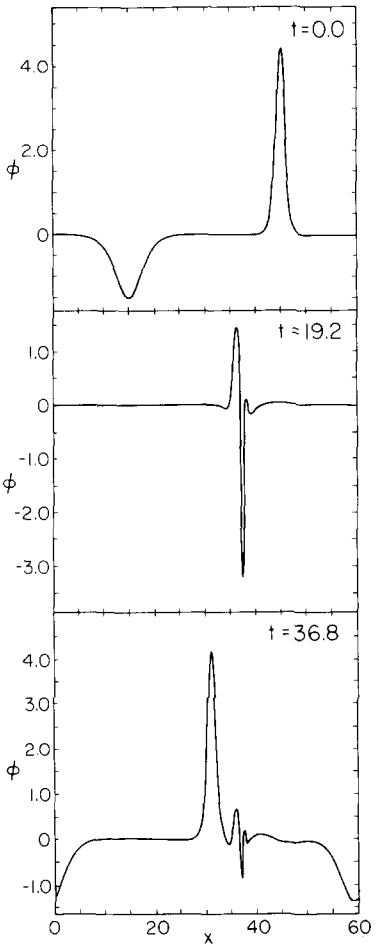

Fig. 8. RLW collision with $c_1 = 1.5$ and $c_2 = -0.5$ showing large amount of radiation.

the center of the collision because of distortion of the waveforms, the phase shift obtained is nearly exact.

When $a_1 a_2 < 0$, the collision is much more violent, as exemplified by the large distortions of waveforms in figs. 5 and 8. The trial function equations attempt to mimic this by having $y \to 0$, but apparently eq. (17) is not general enough. In fig. 11 we see that the trial function trajectories only poorly approximate the actual solution. In particular, the sign of the phase shift is incorrect.

The EWE phase shift exhibits a resonance near $c_2 = -c_1 = -1.5$. This collision is unusual in that $\phi(x, c) = -\phi(x, -c)$ for the EWE and, hence, the total mass and energy are zero. Indeed, in this

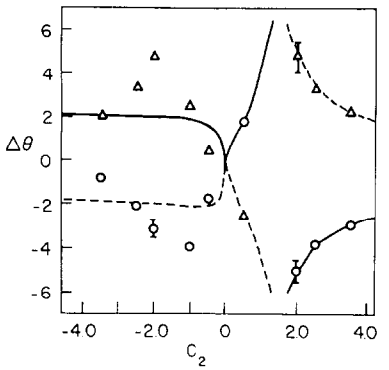

Fig. 9. Phase shifts for EWE with $c_1 = 1.5$. Circles and solid lines represent $\Delta\theta_1$, while triangles and dashed lines represent $\Delta\theta_2$. The curves are obtained from eqs. (40) and (41).

collision it is possible that six or more solitary waves are created. The computation shows that a narrow spike is formed at the collision center and two trains of solitary waves are emitted. Each successive solitary wave has smaller amplitude. At $t - t_c \approx 50$, there are six peaks which are still not separated enough to determine their asymptotic velocities, and it appears that more solitary waves will be created.

Acknowledgements

This work was begun at the Aspen Center for Physics. PJM would like to thank Alan Weinstein for pointing out refs. 6 and 7, and the transformation eq. (45) (which is contained in ref. 6). Support of the DOE through contract DE FG05-80ET-53088 is acknowledged.

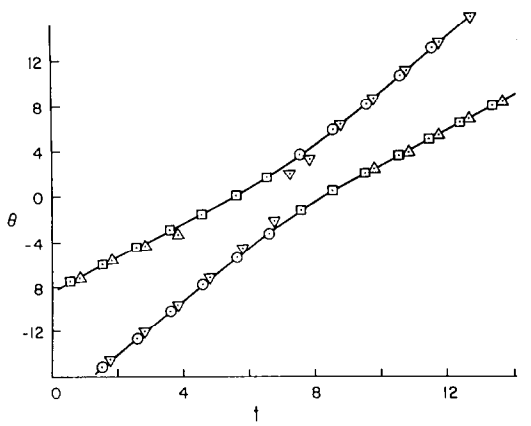

Fig. 10. Comparison of collisions of the EWE (circles and squares), the RLW equation (triangles) and the trial function method of eqs. (40)–(41) (solid curves).

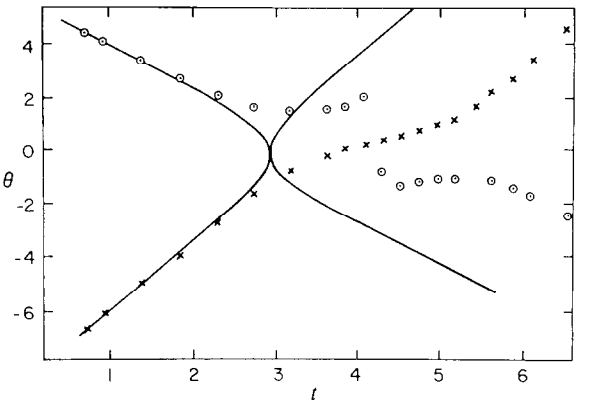

Fig. 11. Trajectories for EWE collision, $c_1 = 2.5$, $c_2 = -1.5$. Circles and crosses designate the position of the solitary wave peaks. The solid curve is obtained from the trial function method.

References

[1] D.H. Peregrine, J. Fluid Mech. 25 (1966) 321.
[2] V. Petviashvili, Sov. J. Plasma Phys. 3 (1977) 150. J.D. Meiss and W. Horton, Phys. Fluids 25 (1982) 1838.
[3] T. Benjamin, J. Bona and J. Mahoney, Phil. Trans. R. Soc. London A272 (1972) 47.
[4] M.D. Kruskal, in: Dynamical Systems, Theory and Applications, J. Moser, ed. (Springer, Berlin, 1976).
[5] K. Abdullov, J. Bogolubsky and V. Makhankov, Phys. Lett. 56A (1976) 427. J.L. Bona, W.G. Pritchard and L.R. Scott, Phys. Fluids 23 (1980) 438.
[6] P.J. Olver, Math. Proc. Camb. Phil. Soc. 85 (1979) 143.
[7] T. Tsujishia, preprint "Conservative Laws of the BBM Equation", (1979).
[8] E.L. Hill, Rev. Mod. Phys. 23 (1951) 253.
[9] R. Courant and D. Hilbert, Methods of Mathematical Physics, vol. I (Wiley, New York, 1953), chap. IV.
[10] F. Tappert, Lect. Appl. Math. 15 (1974) 215.
[11] Dr. T. Kamimura has generously provided us with his program. This algorithm was also used in the 2-D case by M. Makino, T. Kamimura and T. Taniuti, J. Phys. Soc. Jap. 50 (1981) 980.
[12] J.C. Eilbeck and G.R. McGuire, J. Comp. Phys. 23 (1977) 63.
[13] A.R. Santarelli, Nuovo Cimento 46 (1978) 179.
[14] J. Courtenay Lewis and J.A. Tjon, Phys. Lett. 73A (1979) 275.